Instability driven by shear thinning and elasticity in the flow of concentrated polymer solutions through microtubes

Bidhan Chandra,[1] Rahul Mangal,[1] Debopam Das,[2] and V. Shankar[1,*]
[1]*Department of Chemical Engineering, Indian Institute of Technology, Kanpur 208016, India*
[2]*Department of Aerospace Engineering, Indian Institute of Technology, Kanpur 208016, India*

(Received 5 March 2019; published 5 August 2019)

We present a systematic experimental investigation of the onset of instability in the flow of concentrated, shear-thinning, polyethylene oxide (PEO) solutions through rigid microtubes (diameters ∼500 μm and 2840 μm). Micro-PIV measurements are performed for the flow of PEO solutions (∼2000–6000 ppm in water) in the 500 μm tube to obtain the magnitude of normalized velocity fluctuations, which show a jump at Reynolds number Re_s as low as ∼10, indicative of an instability of the laminar flow, where $\mathrm{Re}_s = (DV\rho)/\eta_s$ is the Reynolds number based on the viscosity η_s evaluated at the maximum shear rate prevailing in the flow, D is the tube diameter, V is the cross-sectional average velocity, and ρ is the fluid density. However, the ratio of peak to center-line velocity does not show any significant shift from the laminar value. Experiments are also carried out to obtain friction factor data for the flow of 2000–4000 ppm PEO solutions through a 2.84 mm glass tube. Here the transition is inferred from the deviation of the experimental data from the friction factor associated with the laminar flow obtained by fitting the shear-thinning rheology of the polymer solution using the Carreau model. The data for transition Reynolds number $\mathrm{Re}_{s,t}$ inferred from micro-PIV and friction factor measurements, for polymer solutions of varying concentrations and for two different tube diameters, collapse reasonably well to yield a scaling law $\mathrm{Re}_{s,t} \sim [E_s(1-\beta)]^{-3/4}$, where $E_s = 4\lambda_s\eta_s/\rho D^2$ is the elasticity number based on the fluid relaxation time λ_s estimated at the maximum shear rate of the flow, and β is the ratio of solvent to (shear-rate dependent) total viscosity of the polymer solution. The scaling exponent of $-3/4$ inferred from the present experiments for concentrated polymer solutions is very different from the $-1/2$ exponent reported in previous studies for relatively dilute solutions concerning the onset of elastoinertial turbulence. This suggests that the instability observed in this study for concentrated polymer solutions is qualitatively different from the instability leading to elastoinertial turbulence in relatively dilute solutions. Our study further shows that even rectilinear laminar flows of concentrated polymer solutions become unstable at a relatively low $\mathrm{Re}_s \sim 10$, provided the fluid is both sufficiently shear thinning and elastic.

DOI: 10.1103/PhysRevFluids.4.083301

I. INTRODUCTION

The transition from laminar flow to turbulence in the flow of Newtonian fluids through pipes and channels is dominated by nonlinear effects [1–3], and many fundamental questions underlying this transition continue to be investigated even now. Experiments carried out in the 1970s [4–9] and more recent experiments [10–13] have unambiguously demonstrated that addition of polymers to an otherwise Newtonian fluid can cause early transition in both pipes and channels at Re_0 significantly

*Corresponding author: vshankar@iitk.ac.in

lower than that required for the Newtonian transition. Here Re_0 is the Reynolds number based on the zero shear viscosity, η_0, of the polymer solution. This transition is believed to be caused by both inertial and elastic effects, and hence the term "elastoinertial turbulence" is used to refer to the flow state that ensues this instability. A recent theoretical study [14] has demonstrated that, in sharp contrast to their Newtonian counterparts, tube and channel flows of viscoelastic Oldroyd-B fluids are linearly unstable, and the predictions are in qualitative agreement with experimental observations for the onset of elastoinertial turbulence. This theoretical study has shown that the instability is driven by both inertia and elasticity of the polymer solution and, crucially, is not dependent on the shear-thinning nature of the polymer solution. Experimental investigations on systems with high elasticity numbers (E, defined as the ratio of the solution relaxation time to the viscous diffusion timescale in the flow) exhibit transition at very low Reynolds number [15,16]. This transition, however, is achieved only with perturbed inlet conditions, and the instability is believed to be driven by the elasticity of the polymer solutions because fluid inertia is unimportant at such low Reynolds numbers. Recent experiments by Varshney and Steinberg [17] on the flow of polyacrylamide solutions of relatively low concentrations ~80 ppm, but with very high solvent viscosity (~100 times higher than viscosity of water), in a rectangular channel probed very high elasticity numbers. The channel had two counterrotating cylindrical obstacles, and at low Re, the friction factor for the flow was similar to that for laminar flow of a Newtonian fluid. Beyond a certain $\mathrm{Re} \sim O(1\text{–}10)$, the friction factor deviates from the laminar line, indicating an instability. However, for high elasticity numbers, at a still higher Re, the friction factor again agrees with the laminar prediction suggesting a relaminarization of the flow. The polymer concentrations in all these studies were such that these solutions were weakly shear thinning or nonshear thinning. In the absence of shear thinning, planar shear flows in channels and pipes of viscoelastic fluids are known to be linearly stable (to infinitesimal disturbances) [18–21] at very low Reynolds number, and it is currently believed that nonlinear mechanisms underlie such instabilities [22–24]. At low Re, or in the absence of inertial effects, a linear instability is possible only in viscoelastic flows with curved streamlines. Termed "purely elastic instabilities," these were experimentally observed in curvilinear geometries [25–27] such as Taylor-Couette flow, and the destabilizing mechanism is the "hoop stress" present in curvilinear flows of viscoelastic fluids.

In sharp contrast, recent experimental investigations [28–30] using the flow of highly concentrated polymer solutions reveal that, even for straight geometries with no inlet perturbations, transition can occur at Re_s as low as ~50, if the fluid is sufficiently shear thinning in nature. Here Re_s is the Reynolds number calculated based on the viscosity corresponding to the maximum shear rate in the flow. Also, the posttransition flow behavior was observed to be quite different when compared to that for a Newtonian fluid. Furthermore, theoretical studies by Wilson and co-workers [31–33] have demonstrated the existence of a linear instability, driven by the shear-thinning nature of the polymer solution, even in the absence of fluid inertia. Bodiguel *et al.* [28] investigated the flow of highly shear-thinning partially hydrolyzed polyacrylamide (MW 18×10^6) solution at varying concentrations through rectangular channels of width 152 and 170 μm. It was observed that the flow becomes unstable at very low $\mathrm{Re}_s \sim 10^{-4}$ and $\mathrm{Wi} \sim 6$. Here Wi is defined as the product of the relaxation time of the polymer solution and the maximum shear rate of the flow. The authors argued that the instability is driven by strong shear-thinning nature of the fluid, and hence, it was concluded that inertia had negligible role on the onset of instability. Poole [29] performed laser doppler velocimetry (LDV) measurements for the flow of concentrated, shear-thinning polyacrylamide solutions through channels of half height 12.5 mm and tubes of diameter 100 mm and observed a jump in the normalized velocity fluctuations, a signature of onset of transition, for $\mathrm{Re}_s > 40$, thereby indicating an instability which is driven by the shear-thinning and elastic nature of the fluid. Crucially, the instability was triggered in the absence of any externally imposed perturbations.

Thus, a survey of the experimental literature suggests that instabilities in weakly shear-thinning fluids at very low Re require a finite externally imposed perturbation, but the instabilities in strongly shear-thinning fluids occur spontaneously. In the experiments of Poole [29], while there is a jump in the normalized velocity fluctuations at the onset, which is similar to the Newtonian scenario,

the velocity profile tends to get less flat in the posttransition regime, which is in contrast to the Newtonian transition, wherein a more pluglike behavior is observed. Further, the instability driven by elastic and shear-thinning nature of the polymer solution has been observed for tubes and channels of larger dimensions of $O(100)$ mm, and thus previous studies have probed the regime of relatively low elasticity numbers ~ 0.1.

One of the objectives of the present study is to probe significantly higher values of elasticity numbers (~ 2), by carrying out experiments in tubes of much smaller diameter (~ 0.5 mm) compared to previous studies. Also, the previous study [29] was performed for one polymer concentration, and hence the observations were limited to only one elasticity number. Therefore, a systematic investigation is needed to establish how the instability is affected by the elasticity of the polymer solution. An important question that remains to be addressed is whether the instability leading to elastoinertial turbulence [10] and the instability observed for concentrated solutions [28,29] are distinctly different, or if they are a manifestation of the same instability in different (dimensionless) parameter regimes. In this study, we address this question by carrying out experiments for the flow of concentrated polymer solutions at varying elasticity numbers (by using different concentrations and/or different tube diameters) thereby inferring the scaling law that relates the transition Reynolds number and elasticity number. Previous studies on the onset of elastoinertial turbulence [13] have shown an exponent of $-1/2$ that relates the Reynolds number and the dimensionless product of elasticity number and the ratio of polymer and total solution viscosity, *viz.*, $E(1-\beta)$.

While prior studies have used PIV/LDV measurements to infer the transition in shear-thinning polymer solutions, it is often useful to corroborate the detection of the onset of instability with a different and independent methodology. To this end, in this study, we carry out pressure drop measurements for the flow of 2000–4000 ppm PEO solutions through a 2.84 mm glass tube. To infer the onset of instability, we first compute the expected relation between friction factor f and Re for the laminar flow of a shear-thinning Carreau fluid in a tube. This is then compared with experimental observations, and the Re at which the experimental data deviates from the theoretical laminar prediction is taken to be the onset of transition. We also use dye-stream visualization to corroborate our predictions. Hence, in the present study, we aim to unambiguously detect the onset of the instability in the flow of concentrated polymer solutions through microtubes.

The rest of the paper is organized as follows: Sec. II describes the experimental protocol used; Sec. III describes the micro-PIV observations for the flow of concentrated polymer solution through microtubes; and Sec. IV deals with friction factor measurements and the dye stream visualization experiments to detect the transition. Section V provides a critical discussion of our results, and Sec. VI ends with the salient conclusions of this study.

II. EXPERIMENTAL PROTOCOL

A. Preparation and characterization of PDMS tube

To fabricate tubes of diameters less than 1 mm, we create a tubular bore in a PDMS block as described below. A copper wire is held straight using a screw mechanism, and a well is created by using double sided tapes. A mixture of elastomer base (85%) and cross-linker (15%) is mixed and degassed and then poured into the rectangular well. The PDMS well containing the wire as the template is then cured at 100 °C for 12 h in a preheated oven. After curing, the PDMS block is swelled in toluene for 3 h. The copper wire is then carefully removed from the PDMS block leaving a hollow tubular bore. The PDMS block is then deswelled at low temperature in a refrigerator. The diameter of the bore created is measured using a microscope and a microscale is used for the calibration of the same. This method of preparation of the microtube is similar to the one used in our earlier work [13].

The same PDMS mixture is simultaneously poured in rectangular wells made of microscopic glass slides and cured at 100 °C for rheological characterization. Small-amplitude oscillatory experiments are performed on the rectangular PDMS block to obtain the shear and loss modulus

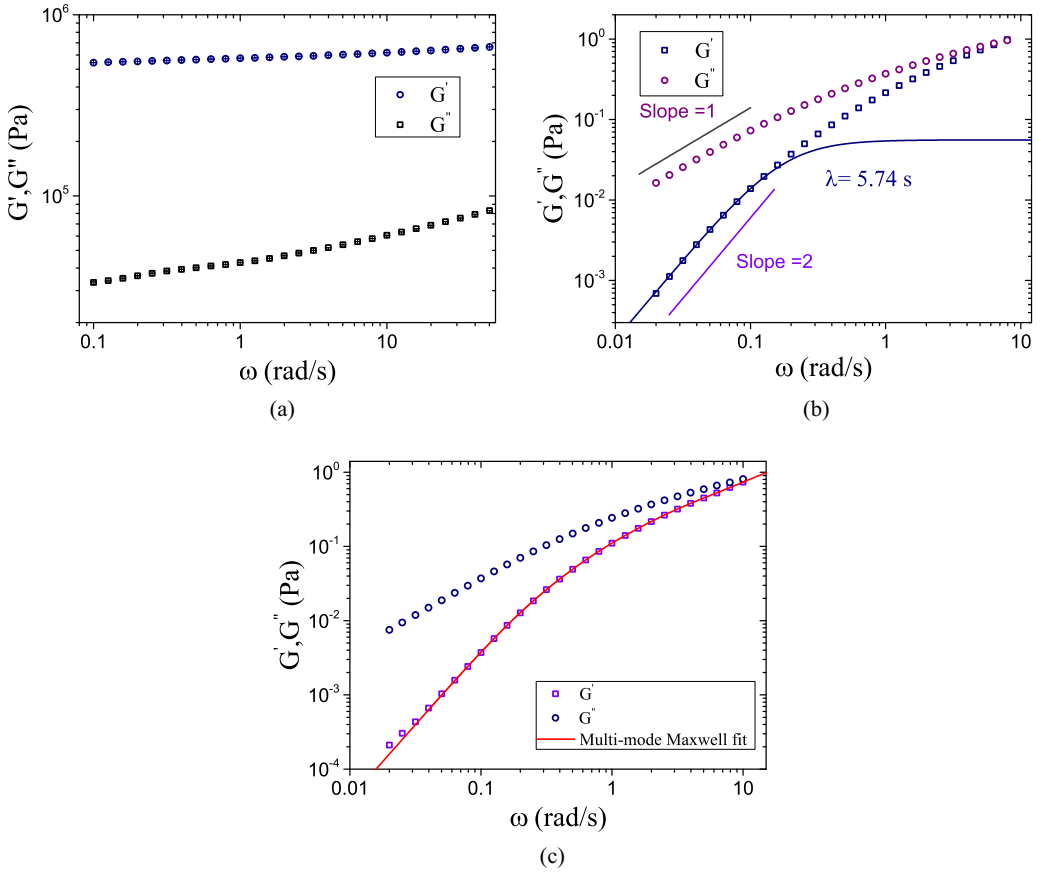

FIG. 1. (a) Shear and loss moduli of PDMS used for tube fabrication. The shear modulus is found to be more than 5×10^5 Pa, and hence the tube wall can be considered as rigid. (b) Shear and loss moduli for 6000 ppm polyethylene oxide solution. The data are fitted to the single-mode Maxwell model to obtain the longest relaxation time of the solution. (c) Fitting of 5000 ppm PEO solution oscillatory data into a multimode Maxwell model. A spectrum of four relaxation times is obtained with $\lambda_1 = 3.33$ s, $\lambda_2 = 1.11$ s, $\lambda_3 = 0.33$ s, and $\lambda_4 = 0.04$ s. Average of the spectrum of relaxation times is 1.2 s.

of the prepared cross-linked PDMS block as shown in Fig. 1(a). It is observed that the shear modulus measured is more than 5×10^5 Pa, and hence the tube can be considered rigid [13,34,35]. For these microtubes we observed that the transition Re_t for the flow of pure water is very close to the well-documented transition Re_t of 2000. For friction factor measurements, a glass tube of 2.84 mm diameter was used. For micro-PIV measurements, a glass tube is not suitable because of the large mismatch in refractive index of glass (RI $\sim$ 1.5) when compared to the fluid refractive index (RI $\sim$ 1.3). The refractive index of PDMS (RI $\sim$ 1.4) is closer to the fluid refractive index and hence is more suitable for micro-PIV measurements.

B. Preparation and characterization of polymer solution

Required amount of polyethylene oxide in powder form (MW 8×10^6) is added to deionized water and the resulting mixture is stirred thoroughly at 25 °C with the help of a magnetic stirrer at 50 rpm for 24–48 h until complete dissolution. Aggregation of PEO solution was observed while mixing the solution. However, the aggregation disappeared after mixing for 24–48 h. The

TABLE I. Rheological properties of various polymer solutions used in the experiments: (concentration-dependent) relaxation time (λ), zero-shear viscosity (η_0), and shear-thinning exponent (n) defined as $\eta \sim \dot{\gamma}^{-n}$.

C_p (ppm)	λ (s)	η_0 (Pa s)	n
2000	0.26	0.022	0.25
3000	0.45	0.077	0.38
4000	1.61	0.25	0.46
5000	2.00	0.45	0.49
6000	5.56	0.90	0.52
6500	9.20	1.95	0.57

beaker is covered with parafilm during the mixing process to avoid evaporation. Viscosity of the prepared solution was measured after shearing. There was no change in the viscosity measured before and after the shearing process, hence it is concluded that there is no shear degradation due to the mixing process. The solution thus prepared is used within 24 h of preparation time. The polymer solution is characterized using a rheometer with a concentric cylinder geometry. Small-amplitude oscillatory shear experiments are performed to obtain the shear and loss moduli of the prepared polymer solution as shown in Fig. 1(b). The data are fitted to a single-mode Maxwell model to obtain the longest relaxation time of the polymer solution. Within the frequency range probed, the data is also fitted using a four-mode Maxwell model, as shown in Fig. 1(c). Table I contains the summary of the various polymer solutions used and their rheological properties. The relaxation time reported in this table is obtained after averaging the data from three different experiments for storage and loss moduli.

C. Shear thinning of polymer solution and purely elastic instability

The polymer solution is characterized by measuring its viscosity using the concentric cylinder geometry of a rheometer. Figure 2 shows the normalized viscosity plots for PEO solutions at

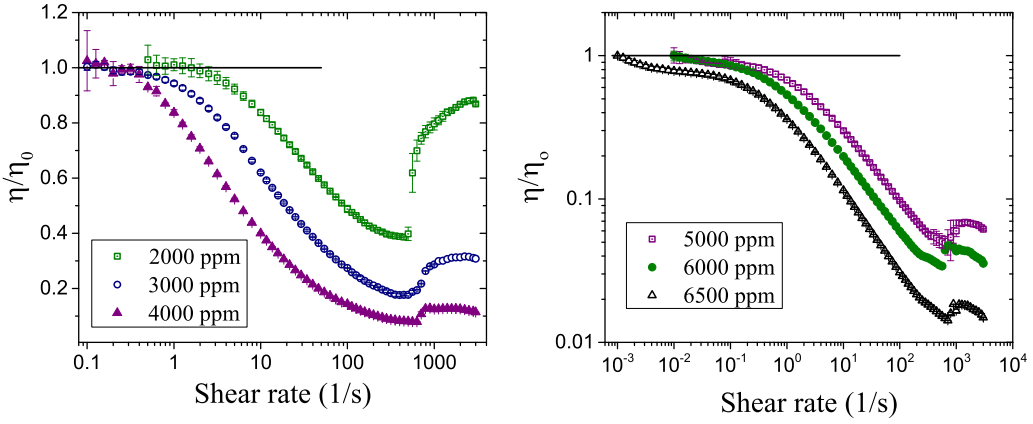

FIG. 2. (a) Normalized viscosity of 2000 ppm, 3000 and 4000 ppm, and (b) normalized viscosity of 5000 ppm, 6000 ppm, and 6500 ppm PEO solutions as a function of shear rate as measured by using the concentric cylinder geometry. η is the shear-rate dependent viscosity of the polymer solution, and η_0 is the zero shear viscosity. The values of η_0 for 2000 ppm, 3000 ppm, 4000 ppm, 5000 ppm, 6000 ppm, and 6500 ppm solutions are 0.022, 0.077, 0.25, 0.45, 0.90, and 1.95 Pa s, respectively.

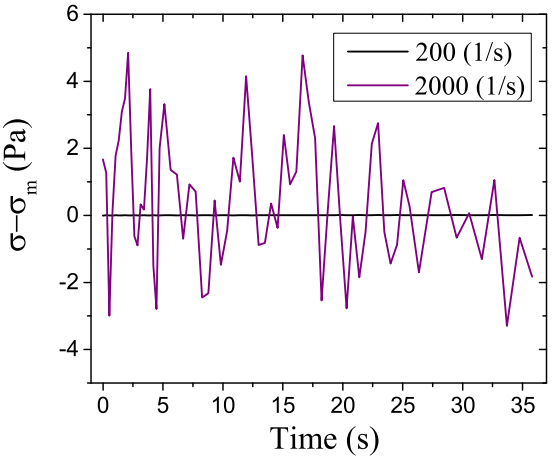

FIG. 3. Comparison of stress fluctuations at low and high shear rates depicting large stress fluctuations in the unstable flow (at high shear rates) of the concentric cylinder flow geometry as compared to the stable regime (at low shear rates). Here σ is the instantaneous stress and σ_m is the mean of stress over time.

different concentrations. The viscosity is normalized with the zero-shear viscosity of the respective polymer solution. It is observed that the solution continuously shear thins up to a certain shear rate, beyond which there is an apparent jump in the measured viscosity. The apparent jump in the polymer viscosity may be attributed to an elastic instability arising due to curved streamlines in the concentric-cylinder geometry [25,26,36]. The Reynolds number for the concentric cylinder geometry is obtained from the expression $[\omega R_1(R_2 - R_1)\rho]/\eta$ where ω is the angular speed, R_1 and R_2 are the diameters of the inner and outer cylinders, ρ is the fluid density, and η is the fluid viscosity, and transition is observed for the concentric cylinder geometry at a Reynolds number $\sim$25. The radii of the inner and outer cylinders are 14 mm and 15 mm, respectively. We observe that the critical Weissenberg number Wi for the onset of instability is Wi $\sim$ 10, where Wi is defined as the product of the shear dependent relaxation time and the shear rate at which the experiment is being performed. We also evaluated the Pakdel-McKinely parameter [37] at the onset of the instability for the concentric cylinder geometry used in our experiments. This parameter turns out to be 3.5 in our case, while the theoretical estimate for the onset [37] is around 8.3. The slight discrepancy between the theoretical and experimental values could be attributed to the uncertainty in inferring the shear-dependent relaxation times at higher shear rates.

Temporal fluctuations in measured stress corresponding to a constant shear rate is a signature of instability in a rheological measurement. We observe that the temporal stress fluctuations is much higher for high shear rates where the flow has become unstable as compared to a lower shear rate where the flow is stable, as measured by the rheometer in a concentric cylinder geometry (Fig. 3). To corroborate the observed phenomena, we compare the measurements of viscosity with varying shear rates using a concentric cylinder geometry and a cone-and-plate geometry. It is observed that the variation of viscosity with shear rate matches for the two geometries up to a certain shear rate, beyond which the concentric cylinder measurements show an apparent jump in the measured viscosity. However, the cone and plate geometry shows a continuous decrease in polymer viscosity with increasing shear rate as shown in Fig. 4(a). This could be because the instability due to curved stream lines might occur at higher shear rates than probed in our experiments.

Since polymer solutions show significant shear thinning with increasing shear rates, the relaxation time of the polymer solution can also be expected to be strongly dependent on the shear rate. To estimate the shear-rate dependence of relaxation time, we measured the first normal stress coefficient using the cone and plate geometry and calculated the shear-rate dependent relaxation time using the

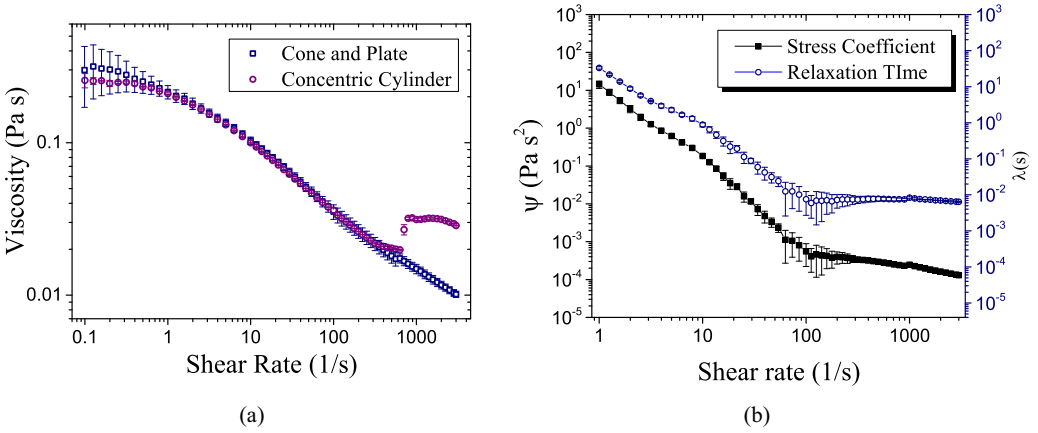

FIG. 4. (a) Comparison of viscosity measured using the concentric cylinder and cone-and-plate geometries for 4000 ppm PEO solution and (b) shear-rate dependent relaxation time calculated using the first normal stress coefficient by using the cone-and-plate geometry. Here the cone angle is 1° and radius is 20 mm.

expression $\lambda = N_1/(\eta\dot{\gamma}^2)$, where λ is the relaxation time, N_1 is the shear-rate-dependent first normal stress difference, η is the fluid viscosity at the relevant shear rate ($\dot{\gamma}$) as shown in Fig. 4(b). Meister and Biggs [38] have shown that the variation of the first normal stress difference with shear rate can exhibit three distinct regions with different slopes. These regions are identified as the diffusion controlled linear region, a regime dominated by the entanglement-disentanglement process, and a third region where aggregation of polymer molecules occurs. An abrupt change in the slope for the first normal stress coefficient occurs when there is a crossover from one regime to another. This change in slope is seen in Fig. 4(b) could be attributed to an onset of entanglement in the solution. Similarly, Ferry [39] also discusses two distinct regimes in the variation of first normal stress difference with shear rate. It is important to quantify the shear-thinning nature of viscosity of the individual polymer solutions. This is estimated by fitting the data in the shear-thinning region using a log-log plot of viscosity versus shear rate. The viscosity varies with shear rate according to the expression $\eta \sim \dot{\gamma}^{-n}$, where n is the magnitude of the shear-thinning slope. In this work, shear rates in the range of 10 s^{-1} to 100 s^{-1} are used to estimate the shear-thinning exponent n. Table I summarizes the key rheological features of the polymer solutions used.

Figure 5 shows the dependence of zero shear viscosity and zero shear relaxation time with the concentration of the polymer used. It is observed that zero shear relaxation time scales with concentration as $\eta_0 \sim c^{3.6}$ and zero shear relaxation time scales with concentration as $\lambda \sim c^{3.7}$. Earlier studies [40,41] have shown that the zero shear viscosity of concentrated polymer solutions scales as $\eta_0 \sim c^{3.4}$. The relaxation time value for 2000 ppm is not included to obtain the scaling relaxation of dependence of zero shear relaxation time with concentration because it is likely that at that concentration the normal stresses in the system might be comparable to the instrument's resolution limits.

III. MICRO-PIV ANALYSIS OF INSTABILITY THROUGH MICROTUBES

For dilute polymer solutions with very high solvent viscosity (i.e., Boger fluids), it is well known that for curved geometries, instability occurs at very low Reynolds number [25,26,36,42,43], which is driven by the hoop stress present in curvilinear viscoelastic flows [26]. However, it is widely believed that the onset of transition in straight tubes and channels occurs only at Re > 500 [10]. Here we carry out micro-PIV analysis to measure the magnitude of normalized velocity fluctuations in the flow of PEO solutions in the microtube of diameter ~540 μm. Use of a smaller

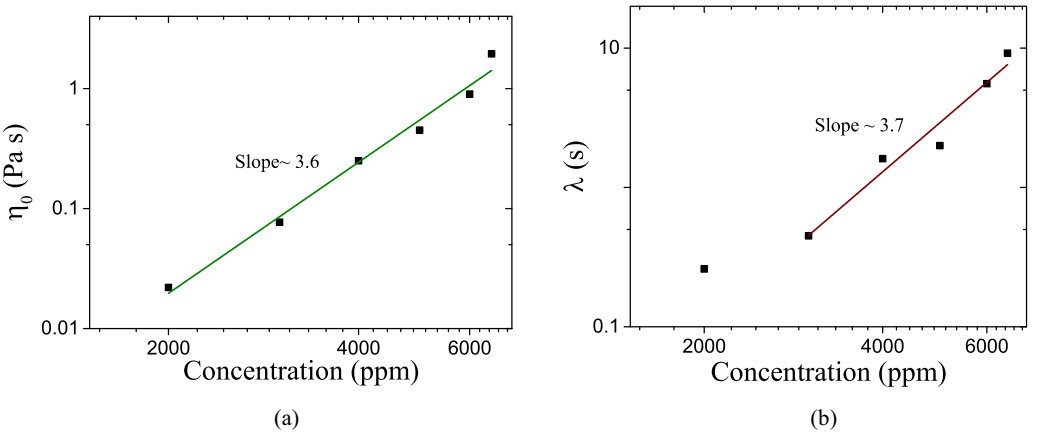

FIG. 5. (a) Dependence of zero shear viscosity on concentration of PEO used. (b) Dependence of zero shear relaxation time on concentration of PEO used.

diameter tube enables us to probe higher values of elasticity numbers $\sim$1. The flow is seeded with fluorescent microspheres of diameter $\sim$3 μm. The Stokes number, St, calculated by the expression $\mathrm{St} = (\rho_p d^2 V)/(18\mu D)$ for the flow experiments is less than 0.1; hence we may assume that the seed particles faithfully follow the fluid streamlines. Here ρ_p is the particle density, d is the particle diameter, V is the cross-sectional average velocity of the tube flow, μ is fluid viscosity, and D is the tube diameter. A laser (15 mJ, Quantel) is used to illuminate the microtube and a CCD camera (Powerview, 8MP) is used for capturing the double-frame images. The time between two frames is kept between 1 and 30 μs. A filter algorithm is used to filter the out-of-plane particles illuminated by the laser. Images are processed using the Insight 4G software which uses a cross-correlation method for getting velocity vectors. The images are processed in two different ways. To obtain the average velocity distribution at various radial locations, the mean instantaneous velocity over a specified time interval is further averaged over three axial locations. The error bar is an indication of the standard deviation in the velocity across the time interval and over the three different axial locations. We also characterize the extent of velocity fluctuations at the center line of the tube. Center-line velocity at a given time instant is calculated by measuring the velocity at different axial locations (at that time instant) of the tube and then taking their average. Then the standard deviation of the center-line velocity at various time instances about their average is obtained. The standard deviation is normalized by the time averaged velocity. The use of center-line velocity for calculating velocity fluctuations minimizes possible errors due to tube curvature and refraction. All micro-PIV measurements are taken 120 diameters away from the tube entrance to avoid any entrance effects. It is further ensured that the polymer solution prepared is used within 24 h of preparation. This is done in order to avoid any degradation in the prepared polymer solution. The temperature in our experiments is maintained at 25 °C.

Figure 6(a) is a comparison of velocity fluctuations obtained for different concentrations as a function of Reynolds number Re_0 based on the zero-shear viscosity of PEO solutions. A jump in the magnitude of normalized velocity fluctuations is considered as an indicator of the onset of transition, and the corresponding Reynolds number is denoted as $\mathrm{Re}_{0,t}$, similar to the earlier experiments of Poole [29]. As already established, the shear-thinning behavior is different for different concentrations of polymer used. It is observed that increasing the concentration of the polymer solution decreases the transition Reynolds number $\mathrm{Re}_{0,t}$. Figure 6(b) is a comparison of velocity fluctuations obtained for different concentrations as a function of Reynolds number Re_s based on the viscosity at the maximum shear rate in the flow. The onset of transition at the corresponding Reynolds number is denoted as $\mathrm{Re}_{s,t}$. Here the maximum shear rate in the tube is

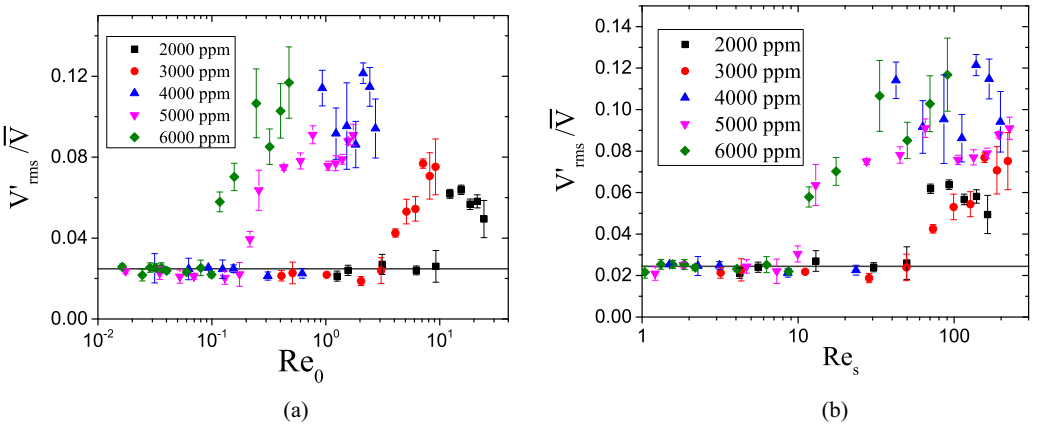

FIG. 6. Onset of instability for PEO solutions of different concentrations: (a) Reynolds number Re_0 is calculated using the zero shear viscosity of the individual PEO solutions. (b) Reynolds number Re_s is calculated using the viscosity corresponding to the maximum shear rate in the flow.

given by $\dot{\gamma} = 8V/D$, where V is the cross-sectional average velocity and D is the tube diameter. Further, the velocity fluctuations monotonically increase after the onset of transition. We also observe that the critical Weissenberg number, Wi_s, at which the normalized velocity fluctuations show a jump in the micro-PIV analysis (and at which the friction factor shows a deviation form the laminar line, as discussed in the following section) varies from $\mathrm{Wi}_s \sim 15$ to $\mathrm{Wi}_s \sim 25$ at the onset of transition for all the concentrations of PEO solutions used in the study. Here $\mathrm{Wi}_s = \dot{\gamma}\lambda_s$, where $\dot{\gamma}$ is the shear rate prevalent in the tube at the corresponding Re_s and λ_s is the relaxation time at the corresponding shear rate. It is interesting to note that earlier observations [29,30] for larger diameter pipes observed similar critical $\mathrm{Wi} \sim 10$. Hence, the transition observed could be due to a combination of the elastic forces and the shear-thinning nature of the polymer solution used as conjectured in Ref. [29]. A comparison of the velocity profile shown in Fig. 7 for laminar (low Re_s) and transitional regimes (high Re_s) for the instability observed illustrates that the posttransition

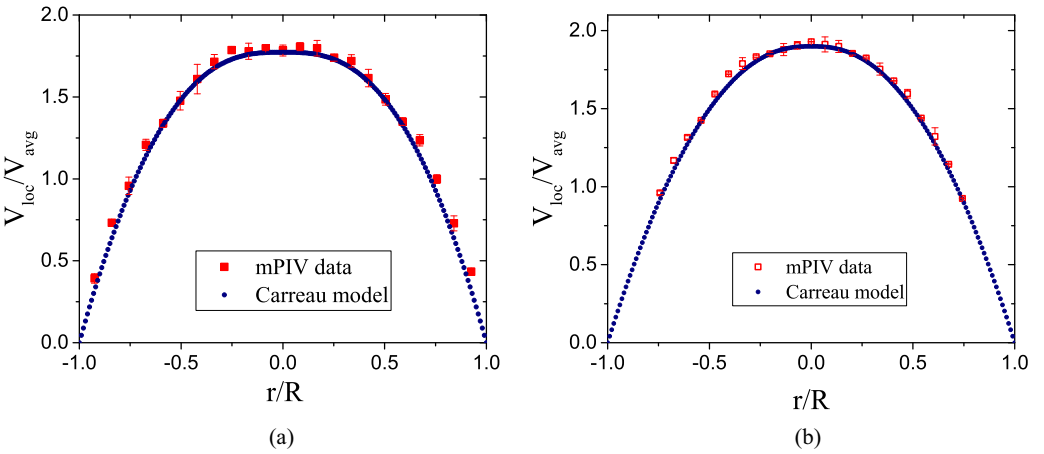

FIG. 7. Comparison of laminar velocity profiles in the laminar and unstable regimes. (a) $\mathrm{Re}_s \sim 1.1$ corresponds to the laminar regime for the flow of 6000 ppm PEO solution, and (b) $\mathrm{Re}_s \sim 90$ corresponds to the unstable regime. V_{loc} is the local velocity, and V_{avg} is the cross-sectional average velocity in the tube.

velocity profile matches with the laminar velocity profile predicted by using the Carreau model for shear-thinning fluids [Fig. 7(b)]. This is in contrast to the Newtonian transition [13,44], where we observe a more pluglike behavior in the turbulent regime. It becomes difficult to obtain data close to the wall owing to the curvature effects near the wall of the microtube.

IV. FRICTION FACTOR MEASUREMENTS FOR THE DETECTION OF THE ONSET OF THE TRANSITION

We obtain the friction factor variation with Reynolds number for the flow of concentrated (2000, 3000, and 4000 ppm) PEO solutions in a glass tube of diameter $D = 2.84$ mm by the measuring pressure drop between a pressure tap located at a distance $\sim 120D$ from the inlet and the tube exit where the pressure is atmospheric. The friction factor is related to the pressure drop as $f = (\Delta P D)/(2LV^2\rho)$, where f is the Fanning friction factor, ΔP is the pressure drop measured across the length, L, V is the cross-sectional average velocity, and ρ is the fluid density. The pressure tap is placed at $120D$ length from the inlet of the tube so as to ensure fully developed flow for pressure measurement. Pressure measurements were first performed for pure water and the Fanning friction factor data obtained matched with the standard friction factor data for the flow through tubes for a Newtonian fluid in both laminar and turbulent regimes.

The laminar f-Re relation for a shear-thinning polymer solution is obtained by using the Carreau model for shear-thinning fluids as described below. The governing momentum equations, under the steady, fully developed, and unidirectional flow assumptions, are solved with the Carreau model for fluid viscosity:

$$\eta = \frac{(\eta_0 - \eta_\infty)}{[1 + (\lambda\dot{\gamma})^2]^{\frac{1-m}{2}}} + \eta_\infty, \tag{1}$$

where η_0 is the zero-shear viscosity, η_∞ is the viscosity at infinite shear rate which is taken as the viscosity of pure water, λ is the relaxation time, and m is the power-law index in the Carreau model. The zero-shear viscosity is taken from our rheological characterization. The governing equations are nondimensionalized using the following scales: η_0 for viscosity, $2V/D$ for strain rate, D for length and displacement, and $f\rho V^2/2D$ for pressure drop. The resulting nondimensional governing equation, after substituting the Carreau model and integrating the momentum equation once, is given by

$$[1 + (2E\mathrm{Re}_s\Gamma^*)^2]^{\frac{m-1}{2}}\Gamma^* = -r^* f\mathrm{Re}_0/16. \tag{2}$$

Here the elasticity number is defined as $E = (\lambda\eta_0)/\rho(D/2)^2$, $\Gamma^* = dV^*/dr^*$ is the nondimensional strain rate, f is the friction factor, m is the power law index, and Re_0 is the Reynolds number based on zero-shear-rate viscosity. For fixed values of Re_0, E, and m, an initial guess of f is provided, and the above equation is used to obtain the local shear rate Γ^* at different radial locations r^*. The velocity profile is then obtained by numerical integration of the local shear rate, from which the (nondimensional) cross-sectional average velocity is computed. Since velocities are made dimensionless using the cross-sectional average velocity, the computed average velocity must be unity if the initial guess for f is correct. We then use a Newton-Raphson method to iterate over the values of f until the dimensionless average velocity becomes unity (within a specified tolerance).

Figure 8 shows a comparison (in the laminar regime) of the velocity profiles obtained from micro-PIV measurements and the theoretical prediction from the Carreau model for the 3000 ppm solution. Here the Carreau model fitting parameters (η_0, η_∞, λ, and m) are taken from rheological measurements. The velocity profile obtained from Carreau model matches very well with that from micro-PIV measurements. Table II shows the fitting parameters used to obtain the laminar friction factor line from Carreau model for shear-thinning fluids. Here the value of E is obtained from rheological measurements and m is used as a fitting parameter to obtain the laminar line for shear-thinning fluids used in our experiments. The shear-rate-dependent viscosity obtained

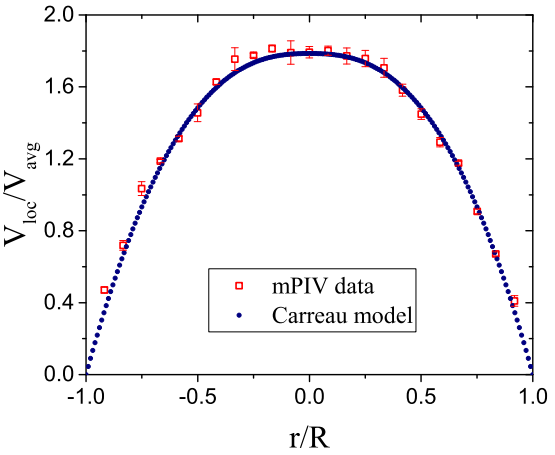

FIG. 8. Comparison of laminar velocity profiles for 3000 ppm PEO solution at $\mathrm{Re}_0 = 0.4$, taken from micro-PIV measurements and from the solution of Carreau model for shear-thinning fluids. V_{loc} is the local velocity and V_{avg} is the cross-sectional average velocity in the tube.

from rheological measurements is used to calculate shear-rate-dependent Re_s. The m and λ values obtained by fitting the rheology data with the Carreau model did not predict the experimentally measured friction factors as accurately as when the parameters of the model are directly fitted to predict the friction factor in the (stable) laminar regime. Our objective below is to infer the onset of instability by carefully looking at deviations from the theoretical (laminar) prediction for the Carreau model, and hence we directly fit the Carreau model constants m and λ to predict the friction factor. For a given m, λ, and E, this procedure is repeated for a range of Re to obtain the f-Re relation for a shear-thinning Carreau fluid.

Figure 9 shows friction factor data for the 2000, 3000, and 4000 ppm PEO solutions as a function of Re for flow through a 2.84 mm glass tube. The deviation in the friction factor data across different runs is very small, and the symbols contain errors bars which in turn are very small to be visible. The friction factor data deviate from the laminar value at $\mathrm{Re}_0 \sim 80$ for 2000 ppm, $\mathrm{Re}_0 \sim 4$ for 3000 ppm, and $\mathrm{Re}_0 \sim 1.5$ for 4000 ppm. Thus, the deviation of friction factor from the expected laminar value further demonstrates the onset of instability in the flow of concentrated polymer solutions. Dye-stream visualization experiments are performed to corroborate the observed instability, with an added objective of demonstrating the instability at a higher polymer concentration. Obtaining pressure drop data for 5000 ppm was quite difficult due to the large response time of the pressure sensor. Hence, we opted to demonstrate the instability at 5000 ppm using dye-stream visualization. A dye stream of diameter $\sim$100 μm is injected into the microtube of diameter 540 μm at the tube inlet. The flow is considered to be laminar if the dye stream appears as a straight line in the microtube [34,35,45], and the break-up of the dye stream is considered to be a signature of

TABLE II. Concentration-dependent relaxation time (λ), Elasticity (E), zero shear viscosity (η_0), shear-thinning exponent from rheology (m_{rheology}), and shear-thinning exponent used for fitting the friction factor data in the laminar regime with the Carreau model (m_{Carreau}).

C_p (ppm)	λ (s)	E	η_0 (Pa s)	m_{rheology}	m_{Carreau}
2000	0.26	2.39	0.022	0.25	0.15
3000	0.45	15.62	0.077	0.38	0.25
4000	1.61	183	0.25	0.46	0.40

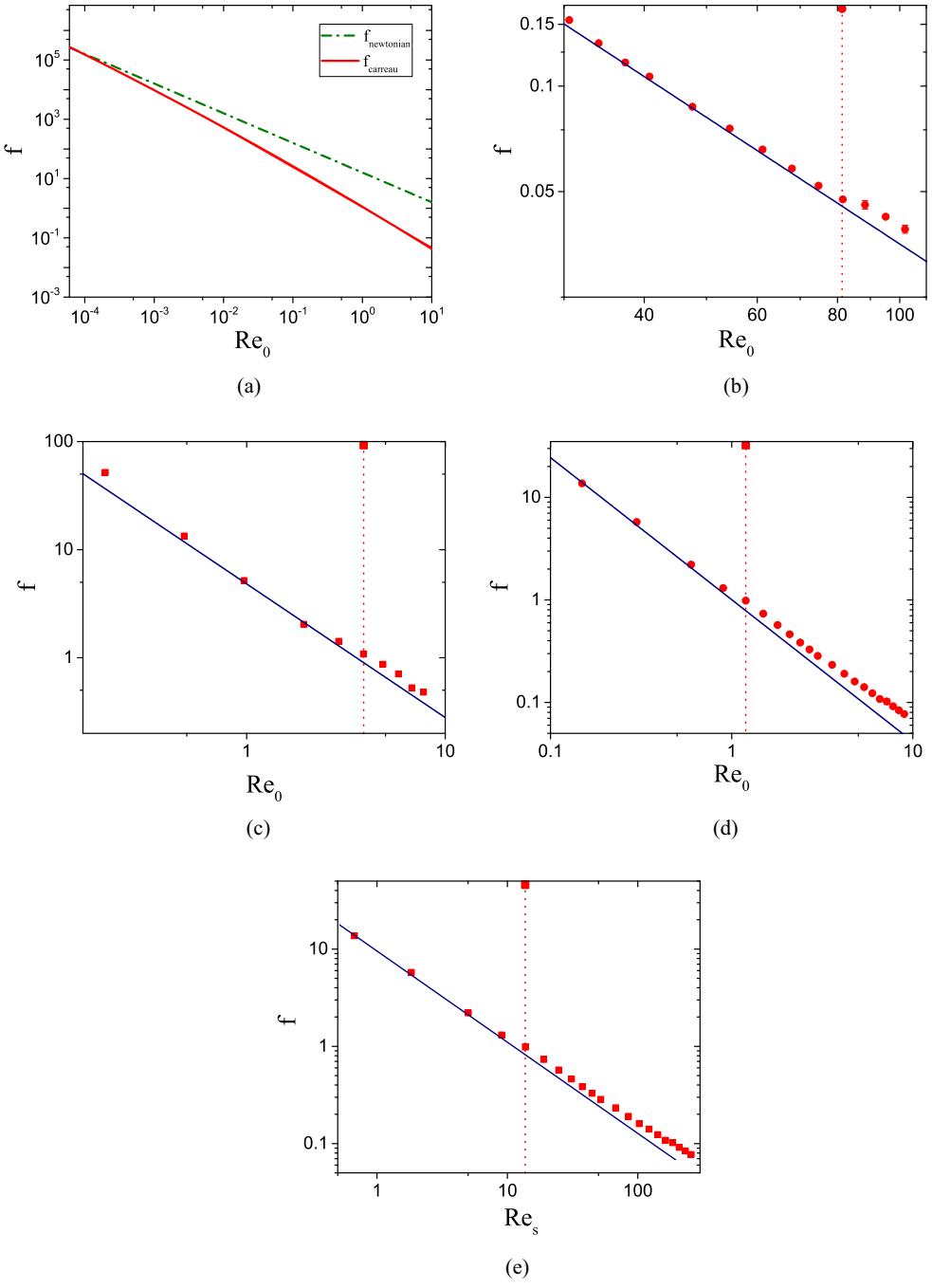

FIG. 9. Friction factor charts for the flow of concentrated PEO solutions through a 2.84 mm glass tube. (a) Laminar friction factor line obtained by using Carreau model, by taking shear-thinning exponent $m = 0.35$ and elasticity $E = 400$, compared with the Newtonian laminar line. (b) Friction factor data for 2000 ppm, (c) 3000 ppm PEO, and (d) 4000 ppm PEO solutions. The solid lines in panels (b), (c), and (d) represent the laminar friction data obtained by using the Carreau model for shear-thinning fluids and dotted vertical line is an indicator of the the onset of transition. (e) Friction factor dependence on Re_s i.e., when Reynolds number is based on the maximum shear rate prevalent in the experiments.

(a)

(b)

FIG. 10. Snapshots of the dye stream visualization experiments in the laminar and posttransition regimes. Dye stream appears as a straight line at $\mathrm{Re}_s \sim 8$ in panel (a), while panel (b) shows the breakage of dye stream at $\mathrm{Re}_s \sim 12$.

the transition. The flow is visualized using a microscope (Olympus, CKX41) and illuminated using a halogen lamp. The microtube is magnified by using a 4× microscope objective. A high-speed camera (IDT, O10) is used to capture images at 1000 fps and 9.2 MP resolution. For a 5000 ppm PEO solution, the dye stream breaks up at $\mathrm{Re}_s \sim 10$ (Fig. 10), which is in close agreement with our micro-PIV results.

V. DISCUSSION

To understand the effect of elasticity of the polymer solution on the instability in pipe flow, experiments are carried out systematically at significantly higher values of elasticity numbers in comparison to previous studies [29]. The nature of instability onset is best understood by investigating how the Reynolds number scales with the elasticity number, as was done for the onset of elastoinertial turbulence at low elasticity numbers in earlier studies [13]. This scaling will also help us to distinguish between the instability observed in this study for concentrated solutions with the onset of elastoinertial turbulence observed in earlier studies for comparatively dilute solutions. When the micro-PIV and friction factor data are plotted for the variation of transition $\mathrm{Re}_{0,t}$ with E_0, respectively, the transition Reynolds and elasticity number based on zero shear viscosity and zero shear relaxation time, a very good data collapse is observed with a scaling law $\mathrm{Re}_{0,t} \sim [(E_0(1-\beta)]^{-0.65}$ as shown in Fig. 11(a). While β is very small for concentrated polymer solutions, we use this factor so as to be consistent with the previous scaling for the onset of elastoinertial turbulence [13]. After correcting for the shear-dependent viscosity and relaxation time, the data corresponds to a scaling of $\mathrm{Re}_{s,t} \sim [E_s(1-\beta)]^{-3/4}$ as shown in Fig. 11(b). Here E_s is the elasticity number defined based on viscosity and relaxation time corresponding to the maximum shear rate in the flow. For the flow of dilute polymer solutions through microtubes, where shear thinning is negligible, and where both inertia and elasticity play an equally important role, the dependence of transition $\mathrm{Re}_{0,t}$ with elasticity number showed a scaling law dependence of $\mathrm{Re}_{0,t} \sim [E_0(1-\beta)]^{-1/2}$ [13]. The substantial difference in scaling exponents for the two instabilities suggests that a qualitatively different mechanism of instability must underlie the transition observed for concentrated, shear-thinning polymer solutions. It is interesting to note that if inertia in the fluid is not important for the observed instability, Re_s should scale as $1/E_s$, since Wi_s will be a constant for such an instability. This is because the fluid density ρ is not a relevant parameter in the absence of inertia. The observed scaling exponent of $-3/4$ (within the dimensionless range of parameters probed here) for concentrated polymer solutions is quite close to the theoretically expected exponent of -1, thus suggesting that fluid inertia may be less relevant to the observed instability, unlike in the case of elastoinertial turbulence, where fluid inertia and elasticity are equally important. More data

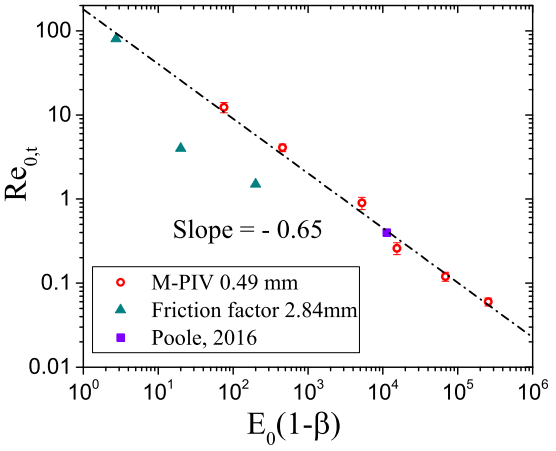

(a)

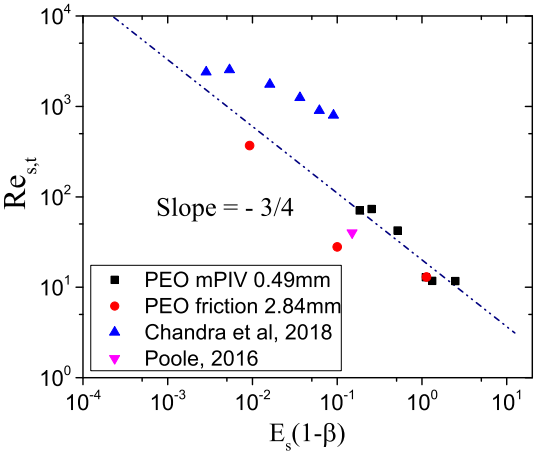

(b)

FIG. 11. (a) Variation of transition Reynolds number, $\mathrm{Re}_{0,t}$, with elasticity number when the Reynolds number is calculated using the zero shear viscosity and (b) transition Reynolds number, $\mathrm{Re}_{s,t}$, with elasticity number when Reynolds number and elasticity number, E_s, are calculated at the maximum shear rates present in the flow. Also shown are results from Poole [29] and Chandra *et al.* [13].

in the range of E lower than those probed in this study are needed to unambiguously determine the exponent in the limit $E \ll 1$.

VI. CONCLUSIONS

In conclusion, in this work, using micro-PIV, friction factor and dye stream visualization experiments, we provide additional evidence of the instability driven by shear thinning and the elastic nature of the fluid, thereby corroborating and augmenting the earlier observations of Refs. [28–30]. By carrying out experiments in tubes of smaller diameters, the present study probes regimes of elasticity numbers much higher than those probed in previous work. Our observations point to the presence of an instability which is qualitatively very different from the Newtonian transition and the elastoinertial transition in relatively dilute polymer solutions. To demonstrate that the observed instability is qualitatively different from the onset of elastoinertial turbulence, we

inferred the scaling relation between the transition Reynolds number and elasticity number, using data from solutions of different polymer concentrations and tubes of two different diameters. This scaling relation is markedly different from that reported for the onset of elastoinertial turbulence and further points to the relatively minor role of fluid inertia in causing this transition. The present results also give rise to some open questions which need to be addressed in future studies. While the shear-thinning nature of the fluid plays a significant role on the onset of instability, the role of elasticity is equally important. Would the instability still persist if the elasticity of the polymer solution is increased without increasing the shear-thinning nature of the fluid, for instance, by using (as in Ref. [17]) relatively dilute solutions in solvents of very high viscosity? A systematic investigation probing such a regime is necessary to obtain a complete understanding of the instability in dilute and concentrated polymer solutions.

ACKNOWLEDGMENTS

The authors thank the Department of Science and Technology, Government of India, for a financial grant (EMR/2016/001218). The authors would also like to thank Ramkarn Patne, Parag Joshi, and Abhishek Ratnam for providing insights and useful suggestions while conducting the experiments.

[1] P. G. Drazin and W. H. Reid, *Hydrodynamic Stability* (Cambridge University Press, Cambridge, 1981).
[2] P. J. Schmid and D. S. Henningson, *Stability and Transition in Shear Flows* (Springer, New York, 2001).
[3] B. Eckhardt, T. M. Schneider, B. Hof, and J. Westerweel, Turbulence transition in pipe flow, Ann. Rev. Fluid Mech. **39**, 447 (2007).
[4] R. J. Hansen, R. C. Little, and P. G. Forame, Experimental and theoretical studies of early turbulence, J. Chem. Eng. Jpn. **6**, 310 (1973).
[5] R. J. Hansen and R. C. Little, Early turbulence and drag reduction phenomena in larger pipes, Nature (London) **252**, 690 (1974).
[6] J. R. A. Pearson, Instability in non-Newtonian flow, Annu. Rev. Fluid Mech. **8**, 163 (1976).
[7] J. L. Zakin, C. C. Ni, R. J. Hansen, and M. M. Reischman, Laser Doppler velocimetry studies of early turbulence, Phys. Fluids **20**, S85 (1977).
[8] J. W. Hoyt, Laminar-turbulent transition in polymer solutions, Nature (London) **270**, 508 (1977).
[9] P. C. Forame, R. J. Hansen, and R. C. Little, Observations of early turbulence in the pipe flow of drag reducing polymer solutions, AIChE J. **18**, 213 (1972).
[10] D. Samanta, Y. Dubief, M. Holzner, C. Schäfer, A. N. Morozov, C. Wagner, and B. Hof, Elasto-inertial turbulence, Proc. Natl. Acad. Sci. USA **110**, 10557 (2013).
[11] A. A. Draad, G. D. C. Kuiken, and F. T. M. Nieuwstadt, Laminar turbulent transition in pipe flow for Newtonian and non-Newtonian fluids, J. Fluid Mech. **377**, 267 (1998).
[12] S. S. Srinivas and V. Kumaran, Effect of viscoelasticity on the soft-wall transition and turbulence in a microchannel, J. Fluid Mech. **812**, 1076 (2017).
[13] B. Chandra, V. Shankar, and D. Das, Onset of transition in the flow of polymer solutions through microtubes, J. Fluid Mech. **844**, 1052 (2018).
[14] P. Garg, I. Chaudhary, M. Khalid, V. Shankar, and G. Subramanian, Viscoelastic Pipe Flow is Linearly Unstable, Phys. Rev. Lett. **121**, 024502 (2018).
[15] D. Bonn, F. Ingremeau, Y. Amarouchene, and H. Kellay, Large velocity fluctuations in small-Reynolds-number pipe flow of polymer solutions, Phys. Rev. E **84**, 045301(R) (2011).
[16] L. Pan, A. Morozov, C. Wagner, and P. E. Arratia, Nonlinear Elastic Instability in Channel Flows at Low Reynolds Numbers, Phys. Rev. Lett. **110**, 174502 (2013).

[17] A. Varshney and V. Steinberg, Drag enhancement and drag reduction in viscoelastic flow, Phys. Rev. Fluids **3**, 103302 (2018).
[18] T. C. Ho and M. M. Denn, Stability of plane Poiseuille flow of a highly elastic liquid, J. Non-Newtonian Fluid Mech. **3**, 179 (1977).
[19] K. C. Lee and B. A. Finlayson, Stability of plane Poiseuille and Couette flow of a Maxwell fluid, J. Non-Newtonian Fluid Mech. **21**, 65 (1986).
[20] M. Renardy and Y. Renardy, Linear stability of plane Couette flow of an upper convected Maxwell fluid, J. Non-Newtonian Fluid Mech. **22**, 23 (1986).
[21] M. Renardy, A rigorous stability proof for plane Couette flow of an upper convected Maxwell fluid at zero Reynolds number, Eur. J. Mech. B **11**, 511 (1992).
[22] B. Meulenbroek, C. Storm, A. N. Morozov, and W. van Saarloos, Weakly nonlinear subcritical instability of viscoelastic Poiseuille flow, J. Non-Newtonian Fluid Mech. **116**, 235 (2004).
[23] A. N. Morozov and W. van Saarloos, Subcritical Finite-Amplitude Solutions for Plane Couette Flow of Viscoelastic Fluids, Phys. Rev. Lett. **95**, 024501 (2005).
[24] A. N. Morozov and W. van Saarloos, An introductory essay on subcritical instabilities and the transition to turbulence in viscoelastic parallel shear flows, Phys. Rep. **447**, 112 (2007).
[25] R. G. Larson, Fluid dynamics: Turbulence without inertia, Nature (London) **405**, 27 (2000).
[26] E. S. G. Shaqfeh, Purely elastic instabilities in viscometric flows, Annu. Rev. Fluid Mech. **28**, 129 (1996).
[27] A. Groisman and V. Steinberg, Efficient mixing at low Reynolds numbers using polymer additives, Nature (London) **410**, 905 (2001).
[28] H. Bodiguel, J. Beaumont, A. Machado, L. Martinie, H. Kellay, and A. Colin, Flow Enhancement due to Elastic Turbulence in Channel Flows of Shear Thinning Fluids, Phys. Rev. Lett. **114**, 028302 (2015).
[29] R. J. Poole, Elastic instabilities in parallel shear flows of a viscoelastic shear-thinning liquid, Phys. Rev. Fluids **1**, 041301 (2016).
[30] C. Wen, R. J. Poole, A. P. Willis, and D. J. C. Dennis, Experimental evidence of symmetry-breaking supercritical transition in pipe flow of shear-thinning fluids, Phys. Rev. Fluids **2**, 031901 (2017).
[31] H. J. Wilson and J. M. Rallison, Instability of channel flow of a shear-thinning White–Metzner fluid, J. Non-Newtonian Fluid Mech. **87**, 75 (1999).
[32] H. J. Wilson and V. Loridan, Linear instability of a highly shear-thinning fluid in channel flow, J. Non-Newtonian Fluid Mech. **223**, 200 (2015).
[33] H. A. Castillo and H. J. Wilson, Towards a mechanism for instability in channel flow of highly shear-thinning viscoelastic fluids, J. Non-Newtonian Fluid Mech. **247**, 15 (2017).
[34] R. Neelamegam and V. Shankar, Experimental study of the instability of laminar flow in a tube with deformable walls, Phys. Fluids **27**, 024102 (2015).
[35] M. K. S. Verma and V. Kumaran, A dynamical instability due to fluid wall coupling lowers the transition Reynolds number in the flow through a flexible tube, J. Fluid Mech. **705**, 322 (2012).
[36] A. Groisman and V. Steinberg, Elastic turbulence in a polymer solution flow, Nature (London) **405**, 53 (2000).
[37] G. H. McKinley, P. Pakdel and A. Oztekin, Rheological and geometric scaling of purely elastic flow instabilities, J. Non-Newtonian Fluid Mech. **67**, 19 (1996).
[38] B. J. Meister and R. D. Biggs, Prediction of the first normal stress difference in polymer solutions, AIChE J. **15**, 643 (1969).
[39] J. D. Ferry, *Viscoelastic Properties of Polymers* (John Wiley and Sons, New York, 1980).
[40] E. Raspaud, D. Lairez and M. Adam, On the number of blobs per entanglement in semidilute and good solvent solution: Melt influence, Macromolecules **28**, 927 (1995).
[41] Y. Heo and R. G. Larson, Universal scaling of linear and nonlinear rheological properties of semidilute and concentrated polymer solutions, Macromolecules **41**, 8903 (2008).
[42] R. G. Larson, E. S. G. Shaqfeh, and S. J. Muller, A purely elastic instability in Taylor-Couette flow, J. Fluid Mech. **218**, 573 (1990).
[43] R. Neelamegam, V. Shankar, and D. Das, Suppression of purely elastic instabilities in the torsional flow of viscoelastic fluid past a soft solid, Phys. Fluids **25**, 124102 (2013).

[44] K. V. Sharp and R. J. Adrian, Transition from laminar to turbulent flow in liquid filled microtubes, Exp. Fluids **36**, 741 (2004).

[45] O. Reynolds, An experimental investigation of the circumstances which determine whether the motion of water shall be direct or sinuous, and of the law of resistance in parallel channels, Proc. R. Soc. London **35**, 84 (1883).